

A dimensionless vent number characterizing the thermal impact of fluid discharge through planar and cylindrical vents with particular application to seafloor gas vents crystallizing hydrate

Lawrence M. Cathles,¹ Duo Fu Chen,^{2,3} and Benjamin F. Nicholson⁴

Received 15 December 2005; revised 19 June 2006; accepted 6 July 2006; published 14 October 2006.

[1] A dimensionless vent number is derived that characterizes the axial temperature changes caused by vertical heat advection in vent zones of planar or cylindrical shape and horizontal dimensions of meters to hundreds of meters or more. The vent number, N_v , depends on the depth extent and width of the vent zone and the rate and duration of venting and is applicable to many common geologic situations such as mud and salt diapirism and gas venting. It provides an easy way to estimate the thermal consequences of venting in cases where the geometry of the vent and its rate and duration of discharge can be estimated. Temperature perturbations are minimal for $N_v < 0.1$. For $N_v > 2$ the temperature profile along the vent zone axis follows the one-dimensional steady state advection profile and horizontal heat losses are negligible. Use of vent numbers is illustrated by assessing the thermal impact of gas venting at the Bush Hill hydrate mound offshore Louisiana. The analysis shows that the temperature perturbations expected from the gas venting there are very small and that any subsurface temperature increase in the area was likely caused by the mud diapirism that preceded the gas venting. The subsurface should be cooling and hydrate crystallizing to progressively greater depths during the ensuing period of gas venting. These conclusions are not obvious but are easily reached using vent numbers.

Citation: Cathles, L. M., D. F. Chen, and B. F. Nicholson (2006), A dimensionless vent number characterizing the thermal impact of fluid discharge through planar and cylindrical vents with particular application to seafloor gas vents crystallizing hydrate, *J. Geophys. Res.*, *111*, B10205, doi:10.1029/2005JB004221.

1. Introduction

[2] The venting of fluids through approximately cylindrical vent zones is a common geological phenomenon. Mud and salt diapirs, and gas vents are cylindrical or tabular in horizontal section. The vertical movement of fluids through these vent zones can perturb subsurface temperatures and produce high surface heat flows. However, the thermal perturbation caused by venting depends on the duration of venting as well as the rate of heat advection in the vent zone and the width and depth extent of the vent zone. There is, at present, no simple way to estimate the conditions under which venting will significantly perturb subsurface temperatures. The purpose of this paper is to present such a

method. We define a vent number analogous to the Peclet number that is used to assess the thermal impact of steady state one-dimensional vertical fluid flow. This vent number combines the duration of venting with the other parameters mentioned above. If the vent number is < 0.1 venting perturbs subsurface temperatures very little. If the vent number is > 2 , subsurface temperatures approach those in one-dimensional (1-D) steady state venting where horizontal heat loss from the vent zone is negligible. We illustrate the use of vent numbers by employing them in an analysis of the temperature impact of seafloor gas vents.

[3] Gas vents are common on the seafloor. In the Gulf of Mexico, most are associated with the faulted margins of salt diapirs [Milkov and Sassen, 2003]. If water depth is greater than ~ 440 m, methane hydrate, an ice-like crystalline mineral in which hydrocarbon and nonhydrocarbon gases are enclosed in a rigid cage of water molecules [Sloan, 1998] may accumulate in the vents [Milkov and Sassen, 2003]. Hydrate accumulations are of current interest because they contain a large volume of natural gas (170 m³ gas per m³ hydrate) that might be exploited [Kvenvolden and Lorenson, 2001], because gas rupturing through a hydrate cap or the rapid decomposition of hydrate can deform the seafloor and trigger mudslides that can impact seafloor infrastructures [Mienert et al., 2005; Maslin et al., 1998],

¹Department of Earth and Atmospheric Sciences, Cornell University, Ithaca, New York, USA.

²Key Laboratory of Marginal Sea Geology, Guangzhou Institute of Geochemistry of Chinese Academy of Sciences, Wushan, Guangzhou, China.

³Gas Hydrate Research Center, Chinese Academy of Sciences, Wushan, Guangzhou, China.

⁴Department of Chemical and Biomolecular Engineering, Cornell University, Ithaca, New York, USA.

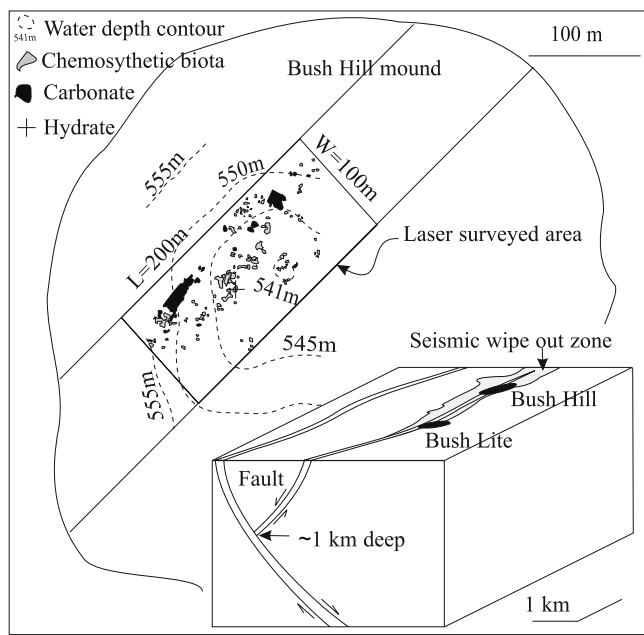


Figure 1. Sketch of gas venting, as it is currently understood, at the ~ 500 m diameter Bush Hill hydrate mound in Green Canyon Block 185, offshore Louisiana, Gulf of Mexico. The hydrate accumulated over the last $\sim 10,000$ years above an antithetic fault spur of the fault system which contains Connoco's Jolliet reservoirs at ~ 1.2 – 2.4 km depth [Cook and D'Onfro, 1991; Roberts and Carney, 1997]. Gas is venting from Bush Hill and Bush Hill Lite where seismic wipe-out zones (shading on top surface of the insert) suggest gas is present near the fault. The most recent venting appears to be localized in a ~ 200 m long interval of a 100 m wide N-S band where the antithetic fault currently cuts across the mound. Two bubble streams a few meters apart near the hydrate outcrop (at plus) on the mound are venting methane at a combined rate of ~ 30 t yr $^{-1}$ [Leifer and MacDonald, 2003]. Mussels, tube worms, and outcrops of hydrate and carbonate mapped by contiguous laser scans [MacDonald et al., 2003] occupy $\sim 3.7\%$ of the 27,650 m 2 area surveyed, as illustrated. These features suggest where gas may have vented in the recent past. De Beukelaer et al. [2003] estimate that up to 10 bubble streams could exist in the laser scanned area.

because hydrate decomposition associated with changes in sea level or ocean temperature could add large volumes of methane (a greenhouse gas) to the atmosphere [Bratton, 1999; Katz et al., 1999; Kennet et al., 2003; Maslin and Thomas, 2003; Kvenvolden and Rogers, 2005], and because hydrate crystallization is an exothermic process that can raise subsurface temperatures. Changes in seafloor temperature affect hydrate stability.

[4] In a previous paper, Chen and Cathles [2005] addressed the thermal impact of broadly distributed gas venting using one-dimensional simulations of venting from 1 km depth that included the latent heat of hydrate crystallization and dissolution above 600 m depth. The 1-D analysis showed that even though the vents may quickly plug with hydrate and be turned off, heat advected by gas

venting and the heat released by hydrate crystallization could cause substantial subsurface warming. The thickness of the hydrate stability zone could be reduced from nearly 600 m to <200 m, and surface temperature gradients increased from 20°C km^{-1} to $>200^\circ\text{C km}^{-1}$, for example. Potentially supporting this analysis, temperature gradients $>400^\circ\text{C km}^{-1}$ have been measured at mud diapers, some of which are venting gas [Ruppel et al., 2005], and erupted mud is often warm [Henry et al., 1996; Eldholm et al., 1999; Wiedicke et al., 2002; Bohrmann et al., 2003; Vanneste et al., 2003; Schmidt et al., 2005]. Here we address whether venting-related temperature perturbations could be produced when the venting is localized. By localized venting we mean that the diameter of upwelling is similar to or smaller than the interval of vertical gas migration.

[5] The issues we address are framed in Figure 1, which depicts gas venting on the 500 m diameter Bush Hill hydrate mound in Green Canyon Block 185, offshore Louisiana, Gulf of Mexico. As evidenced by outcrops of hydrate, mussels, tube worms, and exposed carbonate crust, recent venting appears to have been concentrated where a 100 m wide antithetic fault zone cuts across the ~ 500 m diameter hydrate mound [MacDonald et al., 2003; De Beukelaer et al., 2003]. About half of the fault trace across the mound has been surveyed by contiguous laser scans [MacDonald et al., 2003]. The flow indicators mentioned above occupy $\sim 3.7\%$ of the 27,650 m 2 area that was laser scanned, suggesting venting may be localized even within the surveyed area. In 2001, a bubble stream on a ~ 4 m diameter hydrate outcrop near the center of the mound was venting methane at the rate of a liter per second or 21 t yr $^{-1}$ [Sassen et al., 2001]. Leifer and MacDonald [2003] measured venting rates of a pulsing bubble stream at a hydrate outcrop near the center of the mound in the laser-scanned area (probably the same gas stream measured by Sassen) at 26 t yr $^{-1}$. A steady bubble stream a few meters away was venting at 3.8 t yr $^{-1}$. The combined venting rate of 30 t yr $^{-1}$ is probably the maximum local venting rate on the Bush Hill mound. De Beukelaer et al. [2003] suggest that at most 10 other bubble stream vents of similar magnitude might exist in the laser-surveyed area. If most of the current venting is from the laser-surveyed area and the equivalent of ten ~ 30 t yr $^{-1}$ vents, the total gas venting from the Bush Hill mound would be ~ 300 t yr $^{-1}$. This is similar to the 800 t yr $^{-1}$ estimated by Chen and Cathles [2003] and Chen et al. [2004] from vent chemistry and hydrate crystallization kinetics. A sonar image of the Bush Hill mound shows gas emanating from the full 500 m diameter of the mound [Sassen et al., 2001], not just the surveyed area. This broader distribution of the venting could indicate slow venting across the entire mound, or could be an artifact of the sonar imaging [De Beukelaer et al., 2003].

[6] Figure 1 thus suggests that gas venting could be from a relatively restricted area of the Bush Hill mound. For example, it could be from just a 100×200 m area of the antithetic fault zone that cuts across the mound, or even from a small number of vents a few meters in diameter within this area. The dimensions of these vent areas are much smaller than the gas source depth (which is at least 1 km) and thus restricted in the sense defined above. How

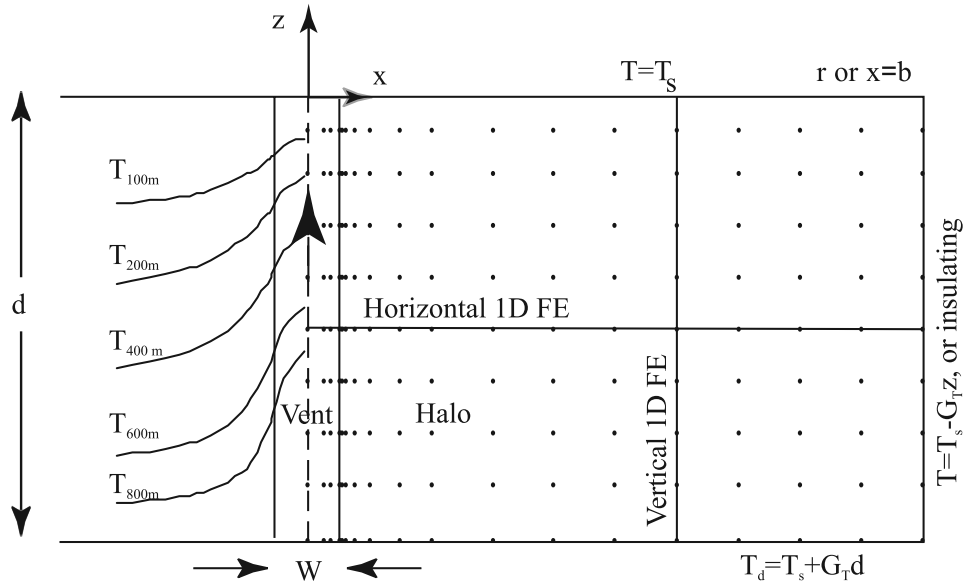


Figure 2. Schematic diagram illustrating aspects of our calculation of the temperature changes caused by gas venting from depth d through a planar or cylindrical vent. The calculation domain is divided into horizontal layers of equal thickness, as indicated by the nodes (dots). At each time step the temperatures at the vent (but not the halo) nodes are moved upward one layer. After each such advection step, the latent heat of hydrate crystallization may be added at the nodes where hydrate is crystallizing, and heat is diffused laterally and vertically by solving the transient 1-D heat flow equation first at each horizontal and then at each vertical line of nodes. The initial temperature at any depth is the normal ambient temperature there. The first node in the sediment adjacent to the vent lies 10 cm from the closest vent node in all cases. The left side of the diagram shows temperature contours away from a typical vent.

much can vertical flow through restricted areas of this nature warm the subsurface?

[7] We address this question semianalytically, following methods derived by *Deloule and Turcotte* [1989] for thin (millimeter wide) cracks. We extend their analysis to include cylindrical as well as planar (fracture) vent zones of meter to hundreds of meter dimensions and show, by comparison to finite element simulations, that their semi-analytical equation of the axial temperature profile in the vent remains a useful measure of subsurface temperature change. We define a new dimensionless “vent” number that in the absence of vertical heat conduction, completely characterizes the axial profile, and we show how this vent number can be used to determine how venting will perturb subsurface temperatures. Applying it to the Bush Hill gas vent site in the Gulf of Mexico, we find that very little subsurface temperature perturbation can be expected from either the very localized gas venting that seems to be occurring at Bush Hill or from venting at plausible rates if the discharge is distributed across the active portion of the mound. On the other hand, significant thermal perturbation should, according to our vent number analysis, commonly be produced by mud diapirism. Increases in subsurface temperatures have been observed near mud diapirs, some of which are venting gas. This suggests that any increase in subsurface temperature or surface heat flow at Bush Hill was caused by mud diapirism, and that the subsurface has

probably been cooling during the period of gas venting that followed mud intrusion.

2. Theory

2.1. An Approximate Solution Assuming No Vertical Conduction

[8] *Deloule and Turcotte* [1989] approximate the temperature perturbations caused by fluid discharge through a narrow vertical fracture assuming vertical heat conduction is negligible. They determine the rate of venting by balancing a lithostatic pressure gradient against turbulent resistance to flow in the narrow planar fracture of width W . They assume turbulent mixing makes the vent isothermal in the horizontal plane. As shown in Figure 2, fluid enters the fracture (which we show as a vent zone of much greater width) at a depth $z = -d$ at the normal temperature for that depth, T_d . For a geothermal gradient G_T , $T_d = T_s + G_T d$. *Deloule and Turcotte* determine the conductive heat losses at the sides of the fracture using the solution for the 1-D transient conduction of heat into a half-space that is initially at the ambient temperature, $T_{amb} = T_s - G_T z$. This is a common assumption [e.g., see *Lowell and Rona*, 2002; *Germanovich et al.*, 2000; *Sleep and Wolery*, 1978]. The conductive heat loss from the walls of the fracture vent is

$$j_h = \frac{K}{\sqrt{\pi \kappa t}} (T_v - T_{amb}). \quad (1)$$

Table 1. Glossary of Parameters With Values Used in Modeling

Symbol	Definition
α	$= \log_{10} t\kappa/r_v^2$
α_d	coefficient of longitudinal dispersion, equal to 30 m
b	distance to lateral boundary [m] (Figure 2)
C	parameter that converts planar vent to cylindrical vent number (see equation (4))
c_f	heat capacity of vent fluid, equal to 4186 J kg ⁻¹ °C ⁻¹ (water), 3000 J kg ⁻¹ °C ⁻¹ (methane gas)
d	depth of vent source below seafloor [m]
δ	thermal conductive skin depth [m], equal to $2\sqrt{\kappa t}$
δ_{adv}	advection skin depth [m], equal to d/N_{Pe}
f_{hyd}	fraction of the gas stream that crystallized as hydrate
ϕ	porosity of sediment, equal to 0.43
G_T	geothermal gradient [°C m ⁻¹]
j_h	horizontal conductive heat loss from side of fracture or cylindrical vent [W m ⁻²]
Q	total mass discharge rate
q_f	vertical mass flux of vent fluid [kg m ⁻² s ⁻¹], equal to $\rho_f V$
K	thermal conductivity of sediment, equal to ~ 1 W m ⁻¹ °C ⁻¹ [Revil and Cathles, 2002]
κ	thermal diffusivity of sediment [m ² s ⁻¹], equal to $K/\rho_m c_m$
L	latent heat of hydrate crystallization, equal to 416,000 J kg ⁻¹ [Rueff et al., 1988]
N_v	dimensionless vent number, $(WN_{Pe}/2d^2)\sqrt{\pi\kappa t}$ in a planar (fracture) vent, and $(r_v N_{Pe}/2d^2 C)\sqrt{\pi\kappa t}$ in a cylindrical vent
N_{Pe}	Peclet number, equal to $\rho_f c_f V d / K$
R_{Tr}	ratio of vent duration, t , to transit time of thermal front across vent, equal to $t/[d/(c_f q_f / \rho_m c_m)]$
r_v	radius of vent in horizontal plane [m]
ρ_f	density of vent fluid [kg m ⁻³], equal to 1000 kg m ⁻³ (water), 38 kg m ⁻³ (methane gas at 54 bars)
$\rho_G c_G$	heat capacity of sediment grains [J m ⁻³ °C ⁻¹], equal to 2.26×10^6
$\rho_m c_m$	heat capacity of sediment [J m ⁻³ °C ⁻¹], equal to $\rho_G c_G (1 - \phi) + \rho_f c_f (\phi)$
S	heat generation by hydrate crystallization or dissolution [J m ⁻³ s ⁻¹], equal to $f_{hyd} q_f L / \Delta z$
T_d	normal (ambient) temperature at a depth d [°C], equal to $T_s + G_T d$
T_s	average seafloor temperature [°C]
T_{amb}	ambient temperature [°C], equal to $T_s - G_T z$
T_v	time-dependent temperature in the vent [°C]
Δt	time required to advect temperature one finite element layer upward, $\Delta z / [(c_f / \rho_f c_f) V]$
V	vertical volume flux of vent fluid [m s ⁻¹]
W	width of fracture [m]
x	horizontal distance [m]
z	depth below seafloor [m], negative down from seafloor
Δz_H	depth to the base of the hydrate stability zone under ambient temperatures [m below seafloor]

Ignoring changes in heat storage in the fracture, Deloule and Turcotte impose heat balance by setting the heat losses out the fracture sides equal to the gradient in vertical heat advection in the fracture. In this way they find the time-dependent temperature in the vent, T_v , depends only on a dimensionless group of parameters that we collect and define here as the vent number, N_v :

$$\frac{T_v(z, t) - T_s}{T_d - T_s} = -\frac{z}{d} + N_v \left(1 - e^{-\frac{z}{N_v d} (z+1)}\right), \quad (2)$$

where

$$N_v = \frac{WN_{Pe}}{2d^2} \sqrt{\pi\kappa t}. \quad (3)$$

N_{Pe} is the Peclet number. The Peclet number is the ratio of the advection of heat in the vent zone to the conductive heat flux in the absence of advection. It is defined in Table 1, as are all other symbols used in this paper. Here the Peclet number provides a measure of the rate of heat advection by vertical flow in the fracture or vent zone.

[9] Deloule and Turcotte's [1989] method can be extended to encompass vertical flow in a cylindrical vent. The Bessel functions expressing radial heat conduction have

been numerically evaluated by Jacob and Lohman [1952]. An expression equivalent to (1) can be written

$$j_h = \frac{CK}{\sqrt{\pi\kappa t}} (T_v - T_{amb}), \quad (4)$$

$$\log_{10} C = 0.2734 + 0.2068\alpha + 0.0316\alpha^2 - 0.0013\alpha^3,$$

where the power series expression for C is the result of a least squares fit we made to Jacob and Lohman's solutions, and $\alpha = \log_{10} t\kappa/r_v^2$. For the cylindrical vent solution, equation (3) becomes

$$N_v = \frac{r_v N_{Pe}}{2d^2 C} \sqrt{\pi\kappa t}, \quad (5)$$

where r_v is the radius of the cylindrical vent. Additional discussion of this and related problems is given by Horner [1951], Bullard [1954], Lee et al. [2003], Chaudhry [2004], Sleep and Wolery [1978], and Carslaw and Jaeger [1959].

[10] Temperature in a horizontally isothermal planar (fracture) vent zone of width W is given by (2) using expression (3) for N_v . Temperature in a horizontally isothermal cylindrical vent zone of radius r_v is given by (2) using expression (5) for N_v .

[11] The remarkable and very useful aspect of equation (2) is that the temperature profile it defines along the axis of a planar or cylindrical vent zone depends on a single parameter, N_v . This parameter combines the depth extent of the vent zone (d), vent zone width (r_v or W), the rate of vertical heat advection in the vent as measured by N_{pes} , and the time the vent has operated (t). Generally, geological observations allow estimation of the geometry of the vent, the venting rate, and the time the vent has operated. Thus N_v can commonly be estimated, and the axial temperature profile predicted from (2). The critical question is whether equation (2) remains valid for the wide vent zones of common geological interest. We show below that it does and that the thermal impact of venting can be inferred from N_v . Subsurface temperatures are not perturbed significantly if $N_v < 0.1$. The temperature profile approaches the maximum possible perturbation (the 1-D steady state vertical advection curve that applies when horizontal heat losses are negligible) when $N_v \sim 2$.

[12] The vent number, N_v , has a simple physical interpretation, which is apparent if the parameters that make up the Peclet Number (see Table 1) are substituted into (5):

$$N_v = \frac{c_f Q}{2\pi d r_v K C} \sqrt{\pi \kappa t} = \frac{r_v \rho_f c_f V}{2d K C} \sqrt{\pi \kappa t}. \quad (6)$$

The vent number is the ratio of the net rate at which heat is advected into the base of the vent at time t , $c_f Q(T_d - T_s)$, to twice the maximum rate at which heat can be conducted from the vent at time t , $2\pi r_v d (CK/\sqrt{\pi \kappa t})[(T_d - T_s)/2]$. Here T_d is the temperature at depth d , and T_s is the temperature at the surface. The maximum rate of heat loss is that from a vent that has temperature T_d everywhere. Its average temperature contrast with ambient is $(T_d - T_s)/2$. The vent will tend toward the 1-D steady state vertical heat advection solution if the advection of heat is greater than the rate at which it can be conducted from the vent, e.g., if N_v approaches or exceeds unity. If the advection of heat into the vent is small compared to the rate at which it can be conducted out the side of the vent, e.g., $N_v \ll 1$, the venting should not perturb subsurface temperatures.

[13] In this paper we use the vent number primarily to assess whether heat advected by the flow of gas through the pores of sediments in a vent zone can produce changes in subsurface temperature. The basic physics is not changed if the heat advection is caused by the penetrative flow of mud or salt through sediments surrounding a diapir. The vent number analysis can thus be used to evaluate thermal perturbations caused by mud or salt diapirs, as we illustrate below.

[14] The vent number is analogous to the Peclet number that characterizes the steady state thermal consequences of the ubiquitous vertical flow of pore fluid from a depth d . It differs from the Peclet Number in that it considers the transient evolution of vent temperature and characterizes the transient thermal effects of vertical flow of fluid in a vent from a depth d . As a time-dependent parameter it is unlike traditional dimensionless numbers in fluid mechanics such as the Peclet or Raleigh numbers that are independent

of space and time, and it is unlikely to play as fundamental a role in fluid mechanics as these numbers. The vent number should be considered a *practical* number that is useful in assessing the thermal impact of venting.

2.2. Finite Element Solutions

[15] *Deloule and Turcotte's* [1989] solution (equation (2)) provides a potentially valuable framework for understanding the thermal effects of venting, but makes a number of assumptions that need to be evaluated, especially when the vent width or diameter becomes appreciable compared to the source depth, d . For example, their method assumes that the horizontal heat conduction was constant over the history of venting to time t (equation (1)), that vertical conductive heat loss is negligible, that the fracture is thin compared to its vertical extent, that the fracture is isothermal in all horizontal planes, and that changes in heat storage in the fracture are not significant. We use standard [Baker and Pepper, 1991] finite element methods in Cartesian and radial coordinates to evaluate whether these assumptions remain valid in much wider vent zones, and to verify our extension of their method to cylindrical vents. We show that changes in heat storage in the vent during the initial stages of venting are not significant, and that the vent number remains a useful characterization of subsurface temperature change even when the vents are neither thin nor isothermal in the horizontal plane, and when vertical heat conduction is important.

[16] Our approach is illustrated in Figure 2. Appealing to symmetry, we model half the system: the midplane of the fracture zone (or the axis of the cylindrical vent zone) is taken to be an insulating plane (or line) across which there is no heat flow. The vent zone sits at the left side of a computation domain whose right boundary may be insulating or fixed at the temperature of the unperturbed geothermal gradient. The fracture (or cylindrical vent zone) and its surroundings are divided into a number (usually 20) of horizontal layers of equal thickness. The nodes are equally spaced vertically, but horizontally their spacing is strongly decreased toward the vent zone margin both in the vent zone itself and in the rock or sediment adjacent to the vent zone which we refer to as the vent halo in Figure 2. Node spacing is defined in Table 2.

[17] We solve the vertical and horizontal heat conduction equations separately and introduce advection at each time step advance of the solution by moving the temperature at each node in the vent up one node (layer). The nodes at the base of the vent at $z = -d$ always have temperature T_d . The time step required for a fluid flux, V , to advect temperature up one layer (assuming no conduction or dispersion of heat) is determined from heat conservation. This time step is $\Delta t = \Delta z / [(\rho_f c_f / \rho_m c_m) V]$, where Δz is the layer thickness. Since the temperatures at each node of the vent are advanced upward exactly to the next node at each time step, there is no numerical dispersion. The first node in the sediment outside the vent lies 10 cm from the closest vent node. This assures accurate definition of the vent width.

[18] After each temperature advection step, heat is diffused for the same interval of time by first solving the transient 1-D lateral heat flow equation at each horizontal line of nodes, and then solving the vertical diffusive heat

Table 2. Parameters Used in Models^a

N_v	W , m	d , m	Δt , years	Q , t yr ⁻¹ m ⁻¹	N_{pe}	q_f , kg m ⁻² yr	δ , m	b , m	R_{TIR}
<i>Fracture of Width W: Comparison to Deloule and Turcotte [1989]: Figure 3a</i>									
0.1	3 (1c, 10h)	1000	2380	5	158	1,670	473	800	8.9
0.1 ^b	3 (1c, 10h)	1000	263	15	476	5,000	315	700	3.0
0.5	3 (1c, 10h)	1000	1653	30	952	10,000	395	500	37
0.5 ^b	3 (4c, 10h)	1000	1653	30	952	10,000	395	500	37
0.5 ^b	3 (1c ⁻ , 10h)	1000	1653	30	952	10,000	395	500	37
0.5 ^b	3 (1c, 10h)	1000	410	60	1904	20,000	196	400	18
0.5 ^b	3 (1c, 10h)	1000	6610	15	476	5,000	790	1500	74
0.5 ^c	3 (1c, 10h)	1000	1613	30	952	10,000	389	800	37
1	3 (1c, 10h)	1000	2380	50	1587	16,667	476	600	89
2.5	3 (1c, 10h)	1000	932	200	1905	66,667	297	600	140
2.5 ^b	10 (1c, 10h)	1000	148	500	4762	50,000	118	300	17
<i>Cylinder of Diameter W: Extension of Deloule and Turcotte [1989] to Cylindrical Vent: Figure 3b</i>									
0.1	3 (1c, 10h)	1000	182	1500	20,210	212,000	131	300	86
0.5	3 (1c, 10h)	500	25	5,000	33,684	707,000	49	150	79
0.5 ^{b,c}	3 (1c, 10h)	500	25	5,000	33,684	707,000	49	150	79
0.5 ^c (a)	200 (40v, 4c ⁻ , 10h)	1000	20,027	13,600	41.2	433	1373	2000	20
0.5 ^{b,c}	200 (20v, 4c ⁻ , 10h)	1000	20,027	13,600	41.2	433	1373	2000	20
0.5 ^{b,c}	200 (20v, 9c ⁻ , 10h)	1000	20,027	13,600	41.2	433	1373	2000	20
0.5 ^c (b)	200 (4c, 10h)	1000	20,027	13,600	41.2	433	1373	2000	20
0.5 ^{c,d} (c)	200 (4c, 10h)	1000	20,027	13,600	41.2	433	1373	2000	20
1	3 (1c, 10h)	400	7	10,000	53,893	1,410,000	26	100	55
2	3 (1c, 10h)	200	7	10,000	26,947	1,410,000	26	100	110
<i>Cylinder of Diameter W: Addition of Vertical Conduction and Dispersion for $N_v = 0.5$: Figure 3c</i>									
0.1 ^c	3 (20v, 1c ⁻ , 10h)	1000	163	1,500	20,210	200,000	124	300	73
0.1 ^c	300 (40v, 4c ⁻ , 10h)	1000	20,095	3,371	4.5	48	1376	2000	2.1
0.5 ^c	3 (20v, 4c ⁻ , 10h)	1000	20	10,309	138,907	1,500,000	43	100	67
0.5 ^c	300 (40v, 4c ⁻ , 10h)	1000	20,010	16,060	21.6	227	1373	2000	10
2 ^c	3 (20v, 4c ⁻ , 10h)	1000	20	56,924	766,968	8,000,000	19	100	358
2 ^c	300 (40v, 4c ⁻ , 10h)	1000	20,007	64,687	87.2	915	1373	2000	41
<i>Cylinder of Diameter W: Steady State 1-D Venting Solution: Figure 4</i>									
0.04	300 (60v, 9c ⁻ , 20h)	1000	>7,785	1,484	2	21	860	3000	0.37
0.24	1000 (60v, 9c ⁻ , 20h)	1000	>11,647	16,493	2	21	1049	3000	0.55
0.63	2000 (60v, 9c ⁻ , 20h)	1000	>11,674	65,973	2	21	1049	3000	0.55
0.63 ^b	2000 (60v, 19c ⁻ , 20h)	1000	>11,674	65,973	2	21	1049	3000	0.55
0.22	300 (40v, 9c ⁻ , 20h)	1000	>15,923	7,420	10	105	1211	3000	3.6
1.08	1000 (40v, 9c ⁻ , 20h)	1000	>7,747	82,470	10	105	860	3000	1.8
2.8	2000 (40v, 9c ⁻ , 20h)	1000	>7,959	329,900	10	105	860	3000	1.8
<i>Cylinder of Diameter W: Thermal Interaction of Adjacent Vents: Figure 5</i>									
0.003	3 (2c, 10h)	1000	20,028	30	404	4,240	1374	30 i	190
0.003	3 (2c, 10h, with hydrate crystallization)	1000	20,028	30	404	4,240	1374	30 i	190
<i>Cylinder of Diameter W: Calculations Specific to Bush Hill: Figure 6</i>									
0.014	100 (4c, 10h)	1000	20,000	300	3.6	38	1372	2,000	1.7

^aSymbols defined in Table 1; (nv, nc, nh) is number of vertical, channel, and halo elements; c⁻ indicates that T in channel nodes not averaged; if number of vertical elements is not given, it is 20; halo nodes spaced progressively 1.5 times farther apart away from vent margin (see Figure 2); channel nodes spaced 0.7 times progressively closer together as vent margin is approached; the first node in the sediment adjacent to the vent lies 10 cm from the closest vent node; i indicates insulating boundary condition.

^bComparison case identical to case plotted.

^cVertical as well as horizontal conduction.

^dDispersion of heat included.

flow equation at each vertical line of nodes (see Figure 2). The equations governing the horizontal diffusion of heat are

$$\rho_m c_m \frac{\partial T}{\partial t} = \frac{\partial}{\partial x} K \frac{\partial T}{\partial x} \tag{7a}$$

$$\rho_m c_m \frac{\partial T}{\partial t} = \frac{1}{r} \frac{\partial}{\partial r} r K \frac{\partial T}{\partial r} \tag{7b}$$

Equation (7a) applies for lateral conduction from a planar vertical fracture, and equation (7b) applies to radial

conduction from a cylindrical vertical vent. The equation governing the vertical diffusion of heat is

$$\rho_m c_m \frac{\partial T}{\partial t} = \frac{\partial}{\partial z} \left(K + \alpha_d \rho_f c_f V \right) \frac{\partial T}{\partial z} \tag{8}$$

Vertical heat dispersion in the vent is accommodated by including the product of the coefficient of longitudinal dispersion, α_d , and the advective heat flux $\rho_f c_f V$.

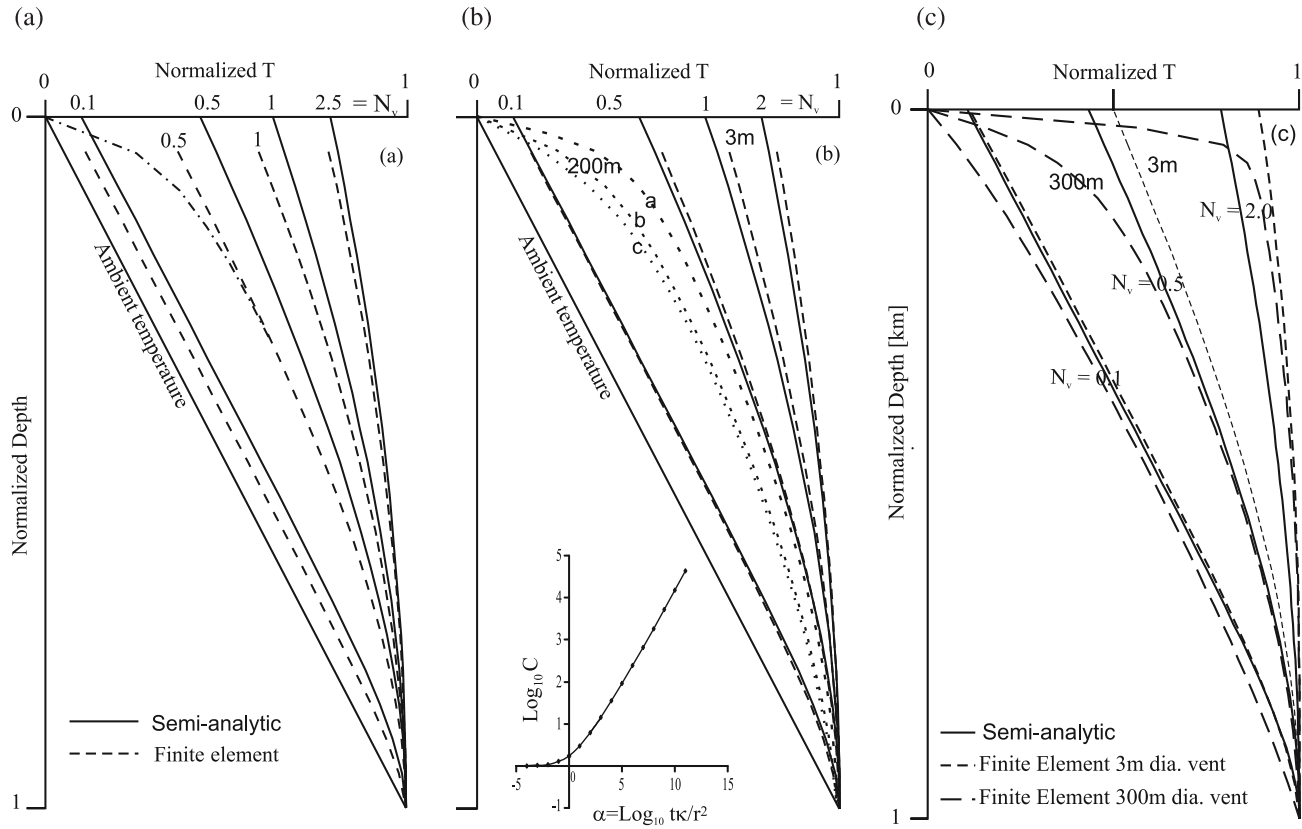


Figure 3. Semianalytic temperature-depth profiles (solid line) calculated using equation (2) compared to finite element simulations (dashed lines) of temperature as a function of depth along the axes of (a) planar (fracture) or (b and c) cylindrical vent zones for a range of N_v values. Vertical heat conduction is calculated for a 3 m wide fracture in the $N_v = 0.5$ cluster of curves in Figure 3a (dot-dashed profile), for three 200 m diameter vents (a, b, c) in the $N_v = 0.5$ cluster in Figure 3b, and for all the finite element curves shown in Figure 3c. Unlike the other profiles where only lateral heat conduction is calculated, the curves where vertical heat conduction is included depend on the dimensions of the vent (not just on N_v). Parameters characterizing each profile are given in Table 2. Together with Table 2, the figure shows that the semianalytic model that depends only on N_v provides a very useful estimate of subsurface temperature change for wide range of vent durations, for wide as well as narrow vents, and for cylindrical as well as fracture vents. Normalized temperature equals $(T_v - T_s)/(T_d - T_s)$, normalized depth equals z/d .

[19] The initial temperature at any depth is the normal ambient temperature there. The temperature at the base is set at T_d , and the surface temperature is set to T_s . The right side may be set to this temperature, or taken as an insulating boundary across which the horizontal temperature gradient is zero. The latter, by symmetry, simulates the thermal impact of adjacent vents.

[20] The temperature of the vent nodes may be averaged laterally after the conduction calculations to simulate, for the purposes of comparison to their model, the turbulent mixing assumed by *Deloule and Turcotte* [1989]. Also the latent heat of hydrate crystallization can be introduced after temperature is advected by raising the temperature at each node where hydrate is crystallizing by $\Delta T = S\Delta t$, where $S = f_{Hyd}q_fL/\Delta z_H$. Here L is the latent heat of hydrate crystallization, and Δz_H is the depth interval over which hydrate is crystallizing (e.g., the thickness of the hydrate stability zone), and f_{Hyd} is the fraction of the gas stream that crystallizes as hydrate between the base of the hydrate stability zone and the seafloor. We assume that the crystal-

lization occurs uniformly from the base to top of this crystallization interval. *Chen and Cathles* [2003] and *Cathles and Chen* [2004] have argued that this could be the case at Bush Hill.

[21] We verified numerical conversion by increasing the number of finite element nodes and time steps, and by carrying out selected finite element simulations where thermal conduction was solved simultaneously in both spatial directions and pore fluid mass flux was specified in the vent zone. For narrow vents it makes little difference if the vent is turbulently mixed (isothermal in the horizontal plane) or not, and 1 vent element is sufficient. For wider vents, with the variable node spacing we use, ~ 4 vent elements are adequate to obtain a converged solution. Convergence results are shown in Table 2 through the comparison of entries with and without an asterisk (*).

2.3. Results

[22] Figure 3 compares the vent axis semianalytic temperature profiles (solid lines) predicted by equation (2) to the profiles computed by finite element methods for the

same N_v values (dashed and dotted lines). Vertical heat conduction is included in the dashed or dotted profiles that reach the surface. These include the dot-dashed line in the $N_v = 0.5$ cluster in Figure 3a, the three dotted curves in Figure 3b that are labeled a, b, c, and all the curves in Figure 3c. The other (dashed) curves do not include vertical heat conduction and are terminated at the first node below the surface. Table 2 gives the parameter values used in the finite calculations shown in this and later figures.

[23] The most important aspect of Figure 3 is its demonstration of how well the semianalytic vent number profiles of equation (2) characterizes the axial finite element temperature-depth profiles in vents zones meters to hundreds of meters in lateral dimension. The semianalytic (solid line) profiles track the finite element profiles (dashed and dotted lines) over the range of N_v values from unperturbed to maximally perturbed subsurface temperatures. The match between the sets of curves for the same N_v is not perfect, but the semianalytic curves are clearly useful as a general guide to the degree of subsurface temperature change.

[24] A perhaps more remarkable aspect of Figure 3 is that each of the dashed or dotted curves actually represents many superimposed curves that are different combinations of vent width, vertical extent, rate of venting, and duration of venting which combine to give the same N_v value. These combinations are given in Table 2 where the cases with overlying curves are indicated by a superscript b. For example the $N_v = 0.5$ dashed curve in Figure 3a depicts venting at $Q = 15 \text{ t yr}^{-1}$ for 6610 years and venting at $Q = 60 \text{ t yr}^{-1}$ for 410 years. In both cases the venting is through a planar fracture zone 1 km in vertical extent and 3 m wide. The two cases have the same N_v value and the curves for the two cases lie on top on one another along the dashed line shown in Figure 3. Similarly, the $N_v = 0.5$ cluster of curves in Figures 3b and 3c show that the semianalytic profile provides a useful measure of subsurface temperature change for cylindrical vents with the same N_v value whether the vents are 3m or hundreds of meters in diameter. The contrasts in the vent characteristics can be stark. In Figure 3c, for example, the 3 m vents have been venting for 20 years, while the 300 m vents have vented for 20,095 years.

[25] A good deal of information is conveyed by Table 2 and Figure 3, and we mention only some highlights. The semianalytic equation (2) profiles match the finite element profiles better, especially for wider vents, if the temperature in the vent is not averaged in the horizontal plane (curve a in Figure 3b), but the agreement is still adequate if the temperatures are horizontally averaged (curve b). Adding a reasonable amount of thermal dispersion ($\alpha_d = 30 \text{ m}$) makes only a small additional change in the finite element profile (curve c). In all but a few cases the amount of heat introduced to the vent zone is large compared to the amount of heat required to warm it, so it is not surprising the initial heating of the vent zone is not a significant omission from equation (2) (see R_{Tr} in Table 2). Table 2 demonstrates convergence. Discussion of some interesting differences between the semianalytic theory and the planar and cylindrical finite element simulations is provided in the appendix.

[26] What is clear from Figure 3 is that the semianalytic profiles of the vent number estimate quite well the changes in subsurface temperature that are caused by venting over a

wide range of venting rates and durations, vent widths and source depths. This indicates that none of the approximations of the semianalytic theory vitiate its usefulness substantially. Figure 3 shows that the transition from virtually no subsurface temperature change to nearly the maximum change possible (ubiquitous steady state 1-D vertical flow in which there is no horizontal heat loss) occurs for $0.1 < N_v < 2$.

[27] Equation (2) is not valid when vertical heat conduction becomes dominant, as will occur when the horizontal dimensions of the vent zone become large compared to the vertical extent of venting. When horizontal conductive heat transport is negligible, the steady state subsurface temperature profile is given [Bredenhoef and Papadopulos, 1965] by

$$\frac{T(z) - T_s}{T_d - T_s} = \frac{e^{N_{pe}z/d} - 1}{e^{N_{pe}} - 1}. \quad (9)$$

For large d , the depth below the seafloor at which temperature reaches 60% of T_b is the advection skin depth, $\delta_{adv} = d/N_{pe}$. Figure 4 shows how temperature changes as a function of vent zone width for a fixed venting rate, q_f , and fixed vertical extent of venting (constant N_{pe}). The finite element profiles in Figure 4 were computed for source depth of 1 km, a gas flux of 21 or 105 $\text{kg m}^{-2} \text{ yr}^{-1}$, and vent diameters of 300, 1000, and 2000 m. Figure 4 shows that for a vent to approach the 1-D steady state profile of equation (9) the vent diameter must be twice the vertical extent of the vent, and N_v must be ~ 2 .

2.4. Application to Cases of Geologic Venting

[28] Table 3 summarizes the characteristics of several kinds of natural vents of cylindrical geometry. Flow modeling [Murton and Biggs, 2003] suggests mud volcanoes vent through cylindrical channels $\sim 9 \text{ m}$ in diameter at remarkably high rates ($\sim 0.8 \text{ m s}^{-1}$). The individual mudflows produced by pulses of mud expulsion cover an area $\sim 1000 \text{ m}$ in diameter and are initially $\sim 3.6 \text{ m}$ thick and $\sim 0.5 \text{ m}$ thick toward the end of mud diapirism. The mud contained at any one instant of time in the diapir vent zone itself could produce a flow with an average thickness of $\sim 0.4 \text{ m}$. Mud volcanoes are known to erupt warm mud, and adjacent heat flow is often high [Henry et al., 1996; Eldholm et al., 1999; Wiedicke et al., 2002; Bohrmann et al., 2003; Vanneste et al., 2003; Ruppel et al., 2005; Schmidt et al., 2005]. The diameter of salt diapirs is often $\sim 10 \text{ km}$ and their rise rate can be as large as 10 mm yr^{-1} [Koyi, 1998; Al-Zoubi and ten Brink, 2001; Ismail-Zadeh et al., 2004]. Table 3 shows that the vent number for mud volcanoes is very high, the vent number for salt diapirs is substantial ($N_v = 0.8$), and the vent number for Bush Hill, discussed earlier, is very low. Both mud and salt diapirs are thus expected to expel hot to warm fluids, and they do. The vent number for the strongest local vent so far observed at Bush Hill (30 t yr^{-1}) is very small ($N_v = 0.003$). Isolated gas venting at Bush Hill should not perturb subsurface temperature.

[29] It can be seen from equation (6) that N_v decreases as the source depth, d , increases. Increasing the radius, r_v , of the vent zone decreases N_v if the total discharge, Q , is kept constant (so a wider zone of local gas venting will diminish

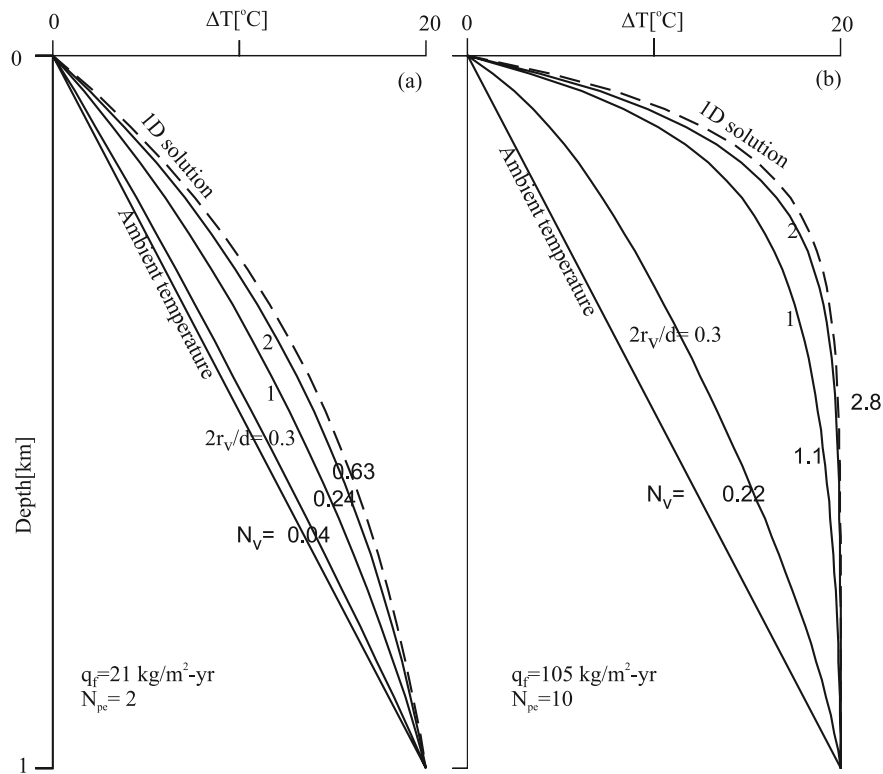


Figure 4. Axial temperature profiles in a cylindrical vent converge to the steady state 1-D vertical flow solution (equation (9)) as the ratio of the vent width to source depth, $2r_v/d$, increases. Results for two specified vertical flow rates in 3 m diameter vents extending to 1 km depth are shown. The duration of venting is $\sim 10,000$ years in all cases. The temperature-depth profile along the vent zone axis approaches the steady state 1-D solution (equation (9) in text) when $W/d > 2$ provided $N_v \sim 2$.

subsurface warming). For a constant diapir rise rate, V , the vent number increases with the radius of the diapir, so wider salt or mud diapirs rising at the same rate will perturb subsurface temperatures more. From (6), and the parameters listed in Table 3, it can be seen that the low mass venting rate, Q , is the main reason that local gas venting at Bush Hill has such a small N_v .

2.5. Further Discussion of the Bush Hill Gas Vents

[30] The conclusion, from Table 3, that gas venting at the highest local rates observed at Bush Hill will not perturb subsurface temperature there is contrary to current perceptions. Are there any circumstances under which venting could warm the subsurface more than indicated by the very low N_v ? Could adjacent vents collaborate to produce greater warming, for example? This possibility is addressed in

Table 3. Vent parameters, Material Properties, and Dimensionless Numbers Characterizing Venting in Selected Geologic Settings^a

Parameter	Bush Hill	Mud Volcanoes	Salt Diapirs
Venting rate Q [kg s ⁻¹]	$9.5 \times 10^{-4} = 30 \text{ t yr}^{-1}$	(9.16×10^4)	(56)
Fluid flux V [m s ⁻¹]	(5×10^{-3})	0.8	$3 \times 10^{-7} = 10 \text{ mm yr}^{-1}$
Vent diameter $2r_v$ [m]	3	9	10,000
Fluid source depth d [m]	1000	4600	5000
Duration of venting [years]	2×10^4	$8 \times 10^{-4} = 7 \text{ hours}$	$>10^5$
Vent fluid heat capacity [J kg ⁻¹ K ⁻¹]	3000	2578	1230
Vent fluid density [kg m ⁻³]	38	1800	2240
Thermal conductivity [W m ⁻¹ K ⁻¹]	1	1	1
Peclet number N_{pe}	404	1.7×10^{10}	4.3
Vent number N_v	3×10^{-3}	280	0.8
Conversion to cylindrical C	112	0.98	1.14
$\sqrt{\pi k t}$	1150	0.15	2090
References	Sassen et al. [2001] and Leifer and MacDonald [2003]	Murton and Biggs [2003]	Al-Zoubi and ten Brink [2001], Ismail-Zadeh et al. [2004], and Koyi [1998]

^aParentheses indicate whether V or Q is the specified parameter.

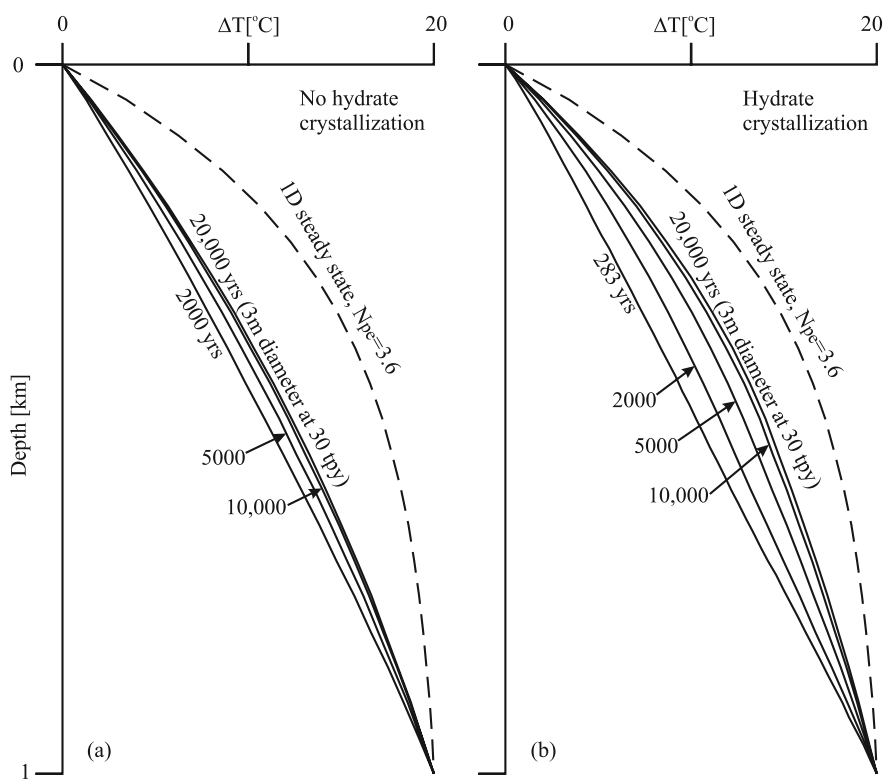


Figure 5. Thermal interaction between an infinite grid of 3 m diameter vents separated by 60 m and discharging gas at 30 t yr^{-1} under 5.4 MPa pressure allowing much greater warming along the axis of each vent than would occur along the axis of a single isolated vent. No axial warming will occur for a single isolated vent of 3 m diameter discharging at 30 t yr^{-1} for 20,000 years because $N_v = 0.003$ for such a vent. An infinite matrix of such vents will warm the subsurface along their axes perceptibly in 20,000 years, however, as shown in Figure 5a. As shown in Figure 5b, the warming will be greater if 10% of the gas stream crystallizes as hydrate between 500 mbsf and the surface. The warming is compared to the steady state warming that would be produced by 1-D vertical flow at the average discharge rate across the vent zone (e.g., 300 t yr^{-1} over the 100 m diameter vent zone). In this case, $N_{Pe} = 3.4$, and the dashed curve computed from equation (9) in the text is the predicted vertical temperature profile. $\Delta T = T - T_s$.

Figure 5. In all the previous finite element simulations the temperature at the boundary away from the vent was set to ambient, and the lateral width of the solution domain was taken to be large enough that the heat flux out the boundary distant from the vent was negligible at the end of the simulation ($b > 2\delta$, see Table 2). In Figure 5 we consider 3 m diameter vents discharging 30 t of gas per year that are separated from one another by 60 m by taking the distant boundary condition to be insulating and the solution domain width 30m. This simulates the heating that would be caused by an infinite grid of 30 t yr^{-1} vents spaced 60 m apart [e.g., *Gringarten et al.*, 1975]. Figure 5a shows how each vent in the infinite matrix of vents will warm along its axis over 20,000 years of venting. Figure 5b shows the additional warming that would be caused by crystallization of 10% of the gas stream as hydrate between 500 m below seafloor (mbsf) and the seafloor. This is the average rate of hydrate crystallization at Bush Hill today [*Chen and Cathles*, 2003]. Figure 5 suggests gas vents could warm the subsurface at Bush Hill significantly.

[31] The subsurface temperature changes at Bush Hill will not be as large as suggested by Figure 5, however, for

two reasons: First the vents will plug with hydrate in ~ 40 years, and the shifting of the vent location will diminish warming. Second, and more importantly, the warming is limited by lateral heat losses from the restricted ($100 \times 200 \text{ m}$) area where the vents occur (e.g., by the finite size of the vent grid).

[32] First consider the plugging time. For a hydrate density of 800 kg m^{-3} , and sediment porosity of 30%, if hydrate fills the pores to a depth of 500 m the vent will contain 120 tons of hydrate in each square meter column between the seafloor and 500 mbsf. A 30 t yr^{-1} gas vent that is 3 m in diameter will crystallize $0.42 \text{ t m}^{-2} \text{ yr}^{-1}$ of gas in hydrate if it loses 10% of its gas to hydrate [*Chen and Cathles*, 2003]. Since hydrate is $\sim 13 \text{ wt } \%$ gas, the vent will crystallize $\sim 3 \text{ t m}^{-2} \text{ yr}^{-1}$ and 120 t m^{-2} in 40 years. Thus the vent will plug with hydrate in ~ 40 years. When the vent plugs it must shift position, and this could retard the heating of the subsurface.

[33] Now consider the lateral heat losses from the entire grid of vents. The actively venting portion of the Bush Hill mound is only about 100 m in diameter (Figure 1) [*MacDonald et al.*, 2003; *Tryon and Brown*, 2004]. Lateral

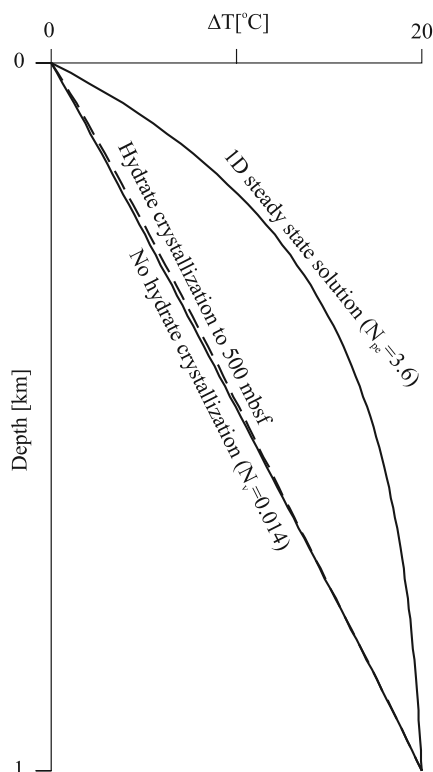


Figure 6. Horizontal heat losses prevent subsurface temperatures from increasing significantly in a 100 m diameter vent discharging at 300 t yr^{-1} ($N_v = 0.014$), even if the latent heat from hydrate crystallization is included. As in Figure 5, the outermost curve is the steady state temperature profile produced by a general gas flux equal that of 300 t yr^{-1} spread over a 100 m diameter area, which gives a Peclet number of 3.6. $\Delta T = T - T_s$.

heat losses from this area will be substantial. Table 2 shows that a 100 m diameter vent discharging at 300 t yr^{-1} through ten 30 t yr^{-1} vents in the area will have a vent number $N_v = 0.014$. Figure 6 shows that gas venting with this vent number will not perturb the subsurface temperature significantly, even if hydrate crystallization contributes heat. Ten vents separated by 60 m would fit in a 200 m diameter area, but venting through a 200 m diameter area would increase the subsurface temperature less than if the same total venting occurred through a 100 m diameter area (equation (6)).

[34] Recently, Tryon and Brown [2004] have measured discrete events of seawater discharge and recharge in the laser-surveyed area shown in Figure 1 that last from 3 to 60 days. They suggest that the water discharge occurs as near-surface gas reservoirs inflate, and that water inflow occurs as the reservoirs deflate. Their largest discharge fluxes occur in areas covered by white bacterial mats. Assuming the flux is the same over the 1500 m^2 area of these mats in the laser-surveyed area, their time series suggest seawater discharges at $\sim 30 \text{ t yr}^{-1}$ for up to ~ 60 days. We are clearly just learning about the complexities of water flow at vent sites such as Bush Hill. From the presently available data, however, the thermal impact of water flow is probably less than that of gas flow and therefore

unimportant to subsurface temperature change. If water vents at 30 t yr^{-1} over the $\sim 100 \text{ m}$ diameter area surveyed about half the time, the discharge rate would be 15 t yr^{-1} , which is much less than the 300 t yr^{-1} gas venting we have considered in our thermal calculations for this same area. The mass discharge rates are appropriate parameters to compare because the heat capacities of the two fluids are similar on a mass basis ($3000 \text{ J kg}^{-1} \text{ }^\circ\text{C}^{-1}$ for gas and $4186 \text{ J kg}^{-1} \text{ }^\circ\text{C}^{-1}$ for water). The periodic inflow of water would tend to cool the subsurface, offsetting the thermal effects of vertical water venting to some degree. Dispersion is likely to cause greater cooling.

[35] It thus seems unlikely that water flow associated with the gas discharge could change our conclusion that gas venting and its associated water flow are not perturbing subsurface temperatures at Bush Hill. We see no way, under the geological constraints we believe pertain at Bush Hill, that gas venting and pore water flow associated with it could warm the subsurface significantly. Many gas vents start as mud diapirs, however, and this is thought to have been the case at Bush Hill. Where this is the case we would expect the subsurface to be appreciably warmed by the mud volcanism. If the venting at Bush Hill is typical, the ensuing gas venting will not sustain the warming, and subsurface temperatures should decrease as gas venting continues. The hydrate stability zone should be deepening, and hydrates should crystallize at progressively greater depths with time. These predictions could provide a basis for testing our analysis. If it is correct, heat flow profiles near hydrate mounds such as Bush Hill may be useful mainly in assessing the time since the last substantial episode of mud diapirism.

3. General Summary

[36] Deloule and Turcotte [1989] developed a semianalytic method for calculating the axial temperature profile in a fracture in which the temperature profile at any time after the initiation of venting is completely characterized by a single parameter, which we call the vent number. This parameter combines the fracture geometry and the duration of venting. In this paper we extended the fracture model of Deloule and Turcotte to include vent zones of cylindrical as well as planar (fracture) geometry and show that their semianalytic method remains useful for vents hundreds of meters or more wide that are not isothermal in the horizontal plane and are subject of vertical conductive heat loss. Vertical heat flow and averaging temperature in the vent impact the Deloule and Turcotte model the most, but even with these additions the vent numbers still characterize the subsurface temperature perturbations in an instructive way, especially for cylindrical vents (Figure 3).

[37] A tremendously useful feature of the semianalytic solution we adapt from Deloule and Turcotte [1989] is that the impact of venting on subsurface temperature depend on a single easily estimated parameter we call the vent number. This single parameter determines whether a vent will significantly modify subsurface temperature and near-surface heat flow. Subsurface temperatures are not perturbed significantly unless $N_v > 0.1$. Fluids will vent close to their source temperatures or lie close to the steady state 1-D Peclet number solution (equation (9)) when $N_v \sim 2$.

[38] The vent number provides a way to estimate subsurface temperature change. The semianalytic equation (2) does not account for a possible difference in thermal conductivity between the vent and its surroundings. A vent may be cylindrical near the surface, but planar at greater depths. The manner in which fluids enter a vent can be important. If one seeks an accurate estimate of advective temperature change in and near a vent, finite element simulations that account for the complexities of the local geology should be constructed. As illustrated in this paper, however, the ability to estimate subsurface temperature using a single “vent” number (equations (3) and (5)) can provide a straightforward method for analyzing quite complex vent and diapir systems. Considering its great simplicity, the vent number method of analysis should be of broad utility.

Appendix A

[39] Figure 3a shows that the finite element (dashed line) profiles along the axis of a planar (fracture) advection zone with no vertical heat conduction are close to the *Deloule and Turcotte* [1989] semianalytic profiles (solid lines) at high and low N_v , but lie substantially on their lower temperature side at intermediate values of N_v . The finite element profiles (dashed lines) we calculate for a cylindrical vent zone with no vertical heat conduction lie (Figure 3b), at intermediate values of N_v , close the semianalytic profiles (solid lines) but always on their high (rather than low) temperature side. These offsets are not significant to the conclusions we reach in the body of this paper, where our interest is to establish that the semianalytical equations provide a good estimate of the subsurface temperature changes caused by venting. The offsets do provide interesting insight to the consequences of approximations made in the semianalytic theory, however, and we discuss this here.

[40] The reason for the different offset of the finite element profiles in the planar advection zone compared to the semianalytic theory of *Deloule and Turcotte* [1989] is the assumption in the semianalytic theory that the heat flux over the history of venting to time t equals the flux at time t (equation (1)). In the 2-D planar (fracture) zone case, the heat flow decreases as $1/\sqrt{t}$, so the semianalytic theory underestimates the amount of heat lost from the fracture. For this reason the finite element profiles fall to the left (lower temperature) side of the semianalytic profiles at intermediate values of N_v . At low values of N_v , both profiles lie along the normal geothermal temperature profile and thus coincide. At large N_v , the advection is so strong that the underestimate of the heat flux in the transient period while the vent is warming is unimportant, and again the profiles coincide.

[41] The semianalytic theory does a better job in the case of cylindrical venting because heat flux from the cylindrical boundary decreases much more slowly. For example, in a planar vent the lateral heat flux at 20,000 years will be one tenth of the flux at 200 years, but for a cylindrical vent, because C increases with the duration of venting, the flux at 20,000 years is more than one third of that at 200 years. The semianalytic profiles should thus lie closer to the finite element profiles, and they do. In fact much of the discrepancy between the semianalytic and finite element profiles

now appears to be due to grid resolution in the vent channel. A coarse grid in the finite element channel reduces the heat flux from the thermally averaged channel, and causes finite element profiles with coarse horizontal grid resolution in the vent to underestimate the heat loss from the vent and lie on the high-temperature side of the semianalytic profiles. The finite element profiles move progressively closer to the semianalytic profiles as the number of nodes in the channel is increased. For example, placing 4 rather than 1 element in the vent in the $N_v = 0.5$ finite element calculation shifts the curve shown in Figure 3b 40% closer to the semianalytic curve. Further refinement of either the horizontal or vertical grid makes little difference, however, and we have no explanation for the slight positive offset that remains. Although it could be interesting to explore its cause further for mathematical insights, it is not significant for our current purposes, and we do not analyze it further.

[42] **Acknowledgments.** We would like to acknowledge the helpful comments of four reviewers (two anonymous) and the Associate Editor. In particular, we thank Bob Lowell for pointing out how useful it would be to provide a physical basis of the vent number and Norm Sleep for drawing our attention to the microfish appendix to his 1978 paper with Wolery and for other helpful comments. Chen acknowledges the supports of the Chinese Academy of Sciences (projects KZCX3-SW-224, GIGCX-04-03) and NSFC (grant 40572071). Funds from the corporate sponsors of the Global Basins Research Network have supported Chen on six visits to the United States, including the one that allowed preparation of this paper. Nicholson is grateful for the support of the Department of Education through a GANN fellowship.

References

- Al-Zoubi, A., and U. S. ten Brink (2001), Salt diapirs in the Dead Sea basin and their relationship to Quaternary extensional tectonics, *Mar. Pet. Geol.*, *18*, 779–797.
- Baker, A. S., and D. W. Pepper (1991), *Finite Elements 1-2-3*, 341 pp., McGraw-Hill, New York.
- Bohrmann, G. M., et al. (2003), Mud volcanoes and gas hydrates in the Black Sea: New data from Dvurechenskii and Odessa mud volcanoes, *GeoMar. Lett.*, *23*, 239–249.
- Bratton, J. F. (1999), Clathrate eustasy: Methane hydrate melting as a mechanism for geologically rapid sea-level fall, *Geology*, *27*, 915–918.
- Bredehoeft, J. D., and I. S. Papadopoulos (1965), Rates of vertical groundwater movement estimated from the Earth's thermal profile, *Water Resour. Res.*, *1*, 325–328.
- Bullard, E. (1954), The flow of heat through the floor of the Atlantic Ocean, *Proc. R. Soc. London, Ser. A*, *222*(1150), 408–429.
- Carslaw, H. S., and J. C. Jaeger (1959), *Conduction of Heat in Solids*, 2nd ed., 510 pp., Clarendon, Oxford, U. K.
- Cathles, L. M., and D. F. Chen (2004), A compositional kinetic model of hydrate crystallization and dissolution, *J. Geophys. Res.*, *109*, B08102, doi:10.1029/2003JB002910.
- Chaudhry, A. (2004), *Oil Well Testing Handbook*, Elsevier, New York.
- Chen, D. F., and L. M. Cathles III (2003), A kinetic model for the pattern and amounts of hydrate precipitated from a gas steam: Application to the Bush Hill vent site, Green Canyon Block 185, Gulf of Mexico, *J. Geophys. Res.*, *108*(B1), 2058, doi:10.1029/2001JB001597.
- Chen, D. F., and L. M. Cathles (2005), On the thermal impact of gas venting and hydrate crystallization, *J. Geophys. Res.*, *110*, B11204, doi:10.1029/2004JB003533.
- Chen, D. F., L. M. Cathles, and H. H. Roberts (2004), The chemical signatures of variable gas venting at hydrate sites, *Mar. Pet. Geol.*, *21*, 317–326.
- Cook, D., and P. D'Onfro (1991), Jolliet Field thrust structure and stratigraphy, Green Canyon Block 184, offshore Louisiana, *Gulf Coast Assoc. Geol. Soc. Trans.*, *41*, 100–121.
- De Beukelaer, S. M., I. R. MacDonald, N. L. Guinasso, and J. A. Murray (2003), Distinct side-scan sonar, RADARSAT SAR, and acoustic profiler signatures of gas and oil seeps on the Gulf of Mexico slope, *GeoMar. Lett.*, *23*, 177–186.
- Deloule, E., and D. L. Turcotte (1989), The flow of hot brines in cracks and the formation of ore-deposits, *Econ. Geol.*, *84*, 2217–2225.

- Eldholm, O., E. Sundvor, P. R. Vogt, B. O. Hjelstuen, K. Crane, A. K. Nilsen, and T. P. Gladchenko (1999), SW Barents Sea continental margin heat flow and Hakon Mosby Mud Volcano, *GeoMar. Lett.*, *19*, 29–37.
- Germanovich, L. N., R. P. Lowell, and D. K. Astakhov (2000), Stress-dependent permeability and the formation of seafloor event plumes, *J. Geophys. Res.*, *105*(B4), 8341–8354.
- Gringarten, A. C., P. A. Witherspoon, and Y. Ohnishi (1975), Theory of heat extraction from fractured hot dry rock, *J. Geophys. Res.*, *80*(8), 1120–1124.
- Henry, P., et al. (1996), Fluid flow in and around a mud volcano field seaward of the Barbados accretionary wedge: Results from Manon cruise, *J. Geophys. Res.*, *101*(B9), 20,297–20,323.
- Horner, D. R. (1951), Pressure build up in wells, in *Proceedings of the 3rd World Petroleum Congress, Section II*, pp. 503–521, World Pet. Congr., The Hague, Netherlands.
- Ismail-Zadeh, A., I. Tsepelev, C. Talbot, and A. Korotkii (2004), Three-dimensional forward and backward modelling of diapirism: Numerical approach and its applicability to the evolution of salt structures in the Pricaspian basin, *Tectonophysics*, *387*, 81–103.
- Jacob, C. E., and S. W. Lohman (1952), Nonsteady flow to a well of constant drawdown in an extensive aquifer, *Eos Trans. AGU*, *33*, 559–569.
- Katz, M. E., D. K. Pak, G. R. Dickens, and K. G. Miller (1999), The source and fate of massive carbon input during the latest Paleocene thermal maximum, *Science*, *286*, 1531–1533.
- Kennet, J. P., K. G. Cannariato, I. L. Henty, and R. J. Behl (2003), *Methane Hydrate in Quaternary Climate Change: The Clathrate Gun Hypothesis*, *Spec. Publ.*, vol. 54, edited by J. P. Kennet et al., 224 pp., AGU, Washington, D. C.
- Koyi, H. (1998), The shaping of salt diapirs, *J. Struct. Geol.*, *20*, 321–338.
- Kvenvolden, K. A., and T. D. Lorenson (2001), The global occurrence of natural gas hydrates, in *Natural Gas Hydrates: Occurrence, Distribution, and Detection*, *Geophys. Monogr. Ser.*, vol. 124, edited by C. K. Paull and W. P. Dillon, pp. 3–18, AGU, Washington, D. C.
- Kvenvolden, K. A., and B. W. Rogers (2005), Gaia's breath-global methane exhalations, *Mar. Pet. Geol.*, *22*, 579–590.
- Lee, J., J. B. Rollins, and J. P. Spirez (2003), *Pressure Transient Testing*, *SPE Textbook Ser.*, vol. 9, 356 pp., Soc. of Pet. Eng., Richardson, Tex.
- Leifer, I., and I. R. MacDonald (2003), Dynamics of the gas flux from shallow gas hydrate deposits: Interaction between oily hydrate bubbles and the oceanic environment, *Earth Planet. Sci. Lett.*, *21*, 411–424.
- Lowell, R. P., and P. A. Rona (2002), Seafloor hydrothermal systems driven by the serpentinization of peridotite, *Geophys. Res. Lett.*, *29*(11), 1531, doi:10.1029/2001GL014411.
- MacDonald, I. R., W. W. Sager, and M. B. Peccini (2003), Association of gas hydrate and chemosynthetic fauna in mounded bathymetry at mid-slope hydrocarbon seeps: Northern Gulf of Mexico, *Mar. Geol.*, *198*, 133–158.
- Maslin, M. A., and E. Thomas (2003), Balancing the deglacial global carbon budget: The hydrate factor, *Quat. Sci. Rev.*, *22*, 1729–1736.
- Maslin, M., N. Mikkelsen, C. Vilela, and B. Haq (1998), Sea-level- and gas-hydrate-controlled catastrophic sediment failures of the Amazon Fan, *Geology*, *26*, 1107–1110.
- Mienert, J., M. Vanneste, S. Bunz, K. Andreassen, H. Haflidason, and H. P. Sejrup (2005), Ocean warming and gas hydrate stability on the mid-Norwegian margin at the Storegga Slide, *Mar. Pet. Geol.*, *22*, 233–244.
- Milkov, A. V., and R. Sassen (2003), Preliminary assessment of resources and economic potential of individual gas hydrate accumulations in the Gulf of Mexico continental slope, *Mar. Pet. Geol.*, *20*, 111–128.
- Murton, B. J., and J. Biggs (2003), Numerical modelling of mud volcanoes and their flows using constraints from the Gulf of Cadiz, *Mar. Geol.*, *195*, 223–236.
- Revil, A., and L. M. Cathles (2002), Fluid transport by solitary waves along growing faults: A field example from the South Eugene Island Basin, Gulf of Mexico, *Earth Planet. Sci. Lett.*, *202*, 321–335.
- Roberts, H. H., and R. S. Carney (1997), Evidence of episodic fluid, gas, and sediment venting on the northern Gulf of Mexico continental slope, *Econ. Geol.*, *92*, 863–879.
- Rueff, R. M., E. D. Sloan, and V. F. Yesavage (1988), Heat capacity and heat of dissociation of methane hydrates, *Am. Inst. Chem. Eng.*, *34*, 1468–1476.
- Ruppel, C., G. R. Dickens, D. G. Castellini, W. Gilhooly, and D. Lizarralde (2005), Heat and salt inhibition of gas hydrate formation in the northern Gulf of Mexico, *Geophys. Res. Lett.*, *32*, L04605, doi:10.1029/2004GL021909.
- Sassen, R., S. L. Losh, L. M. Cathles, H. H. Roberts, J. K. Whelan, A. V. Milkov, S. T. Sweet, and D. A. DeFreitas (2001), Massive vein-filling gas hydrate: Relation to ongoing gas migration from the deep subsurface in the Gulf of Mexico, *Mar. Pet. Geol.*, *18*, 551–560.
- Schmidt, M., C. Hensen, T. Morz, C. Muller, I. Grevenmeyer, K. Wallmann, S. Mau, and N. Kaul (2005), Methane hydrate accumulation in “Mound 11” mud volcano, Costa Rica forearc, *Mar. Geol.*, *216*, 83–100.
- Sleep, N. H., and T. J. Wolery (1978), Egress of hot water from midocean ridge hydrothermal systems: Some thermal constraints, *J. Geophys. Res.*, *83*(B12), 5913–5922.
- Sloan, E. D. (1998), *Clathrate Hydrates of Natural Gases*, 2nd ed., 628 pp., CRC Press, Boca Raton, Fla.
- Tryon, M. D., and K. M. Brown (2004), Fluid and chemical cycling at Bush Hill: Implications for gas- and hydrate-rich environments, *Geochem. Geophys. Geosyst.*, *5*, Q12004, doi:10.1029/2004GC000778.
- Vanneste, M., J. Poort, M. D. Batist, and J. Klerkx (2003), Atypical heat-flow near gas hydrate irregularities and cold seeps in the Baikal Rift Zone, *Mar. Pet. Geol.*, *19*, 1257–1274.
- Wiedicke, M., H. Sahling, G. Delisle, E. Faber, S. Neben, H. Beiersdorf, V. Marchig, W. Weiss, N. von Mirbach, and A. Afiat (2002), Characteristics of an active vent in the fore-arc basin of the Sunda Arc, Indonesia, *Mar. Geol.*, *184*, 121–141.

L. M. Cathles, Department of Earth and Atmospheric Sciences, Cornell University, Snee Hall, Ithaca, NY 14853-1504, USA. (lmc19@cornell.edu)
 D. F. Chen, Key Laboratory of Marginal Sea Geology, Guangzhou Institute of Geochemistry of Chinese Academy of Sciences, Wushan, Guangzhou, Guangdong 510640, China.
 B. F. Nicholson, Department of Chemical and Biomolecular Engineering, Cornell University, Ithaca, NY 14853-1504, USA.